Clim. Past Discuss., 10, 2595–2626, 2014
www.clim-past-discuss.net/10/2595/2014/
doi:10.5194/cpd-10-2595-2014

Climate of the Past Discussions
Open Access

Annual proxy data from Lago Grande di Monticchio (southern Italy) contributing to chronological constraints and abrupt climatic oscillations between 76 and 112 ka

C. Martin-Puertas, A. Brauer, S. Wulf, F. Ott, S. Lauterbach, and P. Dulski

GFZ, German Research Centre for Geosciences, Section 5.2 Climate Dynamics and Landscape Evolution, Telegrafenberg, 14473 Potsdam, Germany

Received: 6 June 2014 – Accepted: 18 June 2014 – Published: 26 June 2014

Correspondence to: C. Martin-Puertas (celia@gfz-potsdam.de)

Published by Copernicus Publications on behalf of the European Geosciences Union.

Abstract

We present annual sedimentological proxies and sub-annual element scanner data from the Lago Grande di Monticchio (MON) sediment record for the sequence 76–112 ka, which, combined with the decadal to centennial resolved pollen assemblage, allow a comprehensive reconstruction of six major abrupt cold and relatively humid spells (MON 1–6) in the central Mediterranean during early phase of the last glaciation. These climatic oscillations are defined by intervals of thicker varves and high Ti-counts and coincide with episodes of forest depletion interpreted as cold and wet oscillations. Based on the independent and slightly revised MON-2014 varve chronology (76–112 ka), a detailed comparison with the Greenland ice-core δ^{18}O record (NGRIP) and northern Alps speleothem δ^{18}O data (NALPS) is presented. Based on visual inspection of major changes in the proxy data, MON 2–6 are suggested to correlate with GS 25–20. MON 1 (Woillard event), the first and shortest cooling spell in the Mediterranean after a long phase of stable interglacial conditions, has no counterpart in the Greenland ice core, but coincides with the lowest isotope values at the end of the gradual decrease in δ^{18}O in NGRIP during the second half of the GI 25. MON 3 is the least pronounced cold spell and shows gradual transitions, whereas its NGRIP counterpart GS 24 is characterized by sharp changes in the isotope records. MON 2 and MON 4 are the longest most pronounced oscillations in the MON sediments in good agreement with their counterparts in the ice and spelethem records. The length of MON 4 (correlating with GS 22) support the duration of this stadial proposed by the NALPS timescales and suggests ca. 500 yr longer duration than calculated by GICC05 and AICC2012, which would confirm a possible underestimation in the ice-core. Absolute dating of the cold spells occurring from 112 to 100 ka (MON 1–3) in the MON-2014 chronology is in good agreement with the GICC05 and NALPS timescales but the younger oscillations (MON 4–6) are ca. 3500 yr younger in Monticchio suggesting a so far not recognized and explicable underestimation of varves within the interstadial interval between MON 3 and MON 4 (corresponding to GI 23–GI 22).

CPD
10, 2595–2626, 2014

1 Introduction

The Earth's climate during the Quaternary is shifting between large glaciations and interglaciations. The transitions between those two climatic modes are of special interest since they provide clues to understand the triggering processes of major and abrupt climate shifts. In the marine realm, the last interglacial period is defined as marine isotope stage (MIS) 5e and dated by astronomical tuning to have lasted ca. 14 000 years (yr) between 130 and 116 thousand years before present (ka). The early glacial period in turn spans marine sub-stages MIS 5d-a, which reflect alternation of increased (MIS 5d and b) and reduced (MIS 5c and a) global ice volume (Shackleton, 1987). Based on pollen evidence and varve counting from the sedimentary record of Lago Grande di Monticchio, in southern Italy, the last interglacial is defined from 127.2 to 109.5 ka and thus has lasted a few thousand years longer (17 700 yr) (Bruaer et al., 2007). In northwestern Europe, the last interglacial is biostratigraphically defined as Eemian and characterized by forest dominance, which is thought to broadly correlate with MIS 5e (Harting, 1874). The onset of glacial conditions (Weichselian) following the Eemian was characterized by forest depletion and dominance of open vegetation and has been correlated with MIS 5e/d boundary (~ 115 ka) (Kukla et al., 2002). The Greenland ice-core stratigraphy based on the oxygen isotopes record (NGRIP δ^{18}O record) reveals a gradual temperature decrease since the isotope peak at 122 until 115 ka, suggesting the end of the last interglacial conditions did not occur abruptly in Greenland (Andersen et al., 2004). The period of initial built-up of the Northern Hemisphere ice sheets (early glaciation) was interrupted by recurrent phases of ice retreat (Mangerud et al., 1998). In the NGRIP record these periods of waxing and wining of ice sheets are mirrored by abrupt climate changes between relatively warm and humid Interstadials (GI 20–25) and cold and dry Stadials (GS 26–20) (Andersen et al., 2004). A recent oxygen isotope record from stalagmites in the northern Alps (NALPS) (Boch et al., 2011) revealed rapid temperature changes superimposed on millennial-scale similar to those shown in NGRIP. In addition, shorter warm and cool intervals superim-

CPD
10, 2595–2626, 2014

posed to millennial-scale variability were identified in both NGRIP and NALPS (Capron et al., 2010; Boch et al., 2011). Sea surface temperatures reconstructed for the central-eastern North Atlantic also show millennial-scales climate variability consisting of cold pulses (C25–20) and warm episodes (W24–20) throughout MIS 5d-a (McManus et al., 1994; Sánchez Goñi et al., 1999; Shackleton et al., 2002). In central Europe, vegetation changes recorded in La Grande Pile lake sequence, also describe millennial-scale variability from ~ 111 ka alternating stadials periods (i.e., Woillard event, Melisey 1 and 2 and Montaigu event) and interstadials stages (i.e., St. Germain 1 and St. Germain 2) (Kukla, 1997). In southern Europe, these oscillations have been also recorded in the pollen record from Lago Grande di Monticchio, in Italy (Allen et al., 1999; Brauer et al., 2007) and in the stalagmite record from Corchia Cave, in central Italy (Drysdale et al., 2007).

Establishing teleconnections between the Mediterranean and polar regions from high-resolution records is crucial for a better understanding of millennial- and shorter-scale climate variability during the phase of ice sheet build-up in the Northern Hemisphere. However, there are still only few high-resolution records available and dating uncertainties remain rather large. Despite major attempts to improve ice-core chronologies (e.g., Landais et al., 2006; Capron et al., 2010; Wolff et al., 2010; Vallelonga et al., 2012; Bazin et al., 2013; Veres et al., 2013) dating differences of several millennia are still evident (Veres et al., 2013).

The sediment record from Lago Grande di Monticchio (MON) is the only lake record with an annual resolution and an independent chronology for the early last glacial period based on varve counting, tephrochronology and $^{40}Ar/^{39}Ar$ dating of tephra layers (Allen et al., 1999; Brauer et al., 2000, 2007; Wulf et al., 2004, 2012). However, still today the main focus of investigations has been on vegetation changes at decadal to centennial resolution (Allen et al., 1999; Brauer et al., 2007). In this study we present, for the first time, varve micro-facies and thickness analyses in combination with high-resolution XRF-element scanning data in order to reconstruct the Mediterranean climate variability at annual resolution for the interval 76–112 ka. This enables a high res-

CPD
10, 2595–2626, 2014

olution comparsion of the MON sediment record with the isotope records from Greenland (NGRIP) and the northern Alps (NALPS) and an attempt at proving or disproving possible regional differences between Greenland, the Alps and the central Mediterranean.

2 Regional setting

Lago Grande di Monticchio (MON) (40°56′ N, 15°35′ E, 656 m a.s.l.) is located in the Basilicata region of southern Italy, approximately 280 km Southeast of Rome and 120 km East of Naples. The lake is the largest of two adjacent maar lakes within a caldera on the western slope of Monte Vulture, a Quaternary volcano in the Roman Co-magmatic Province, and was formed at 132 ± 12 ka during the final phreatomagmatic eruptions of Monte Vulture (Brocchini et al., 1994; Stoppa and Principe, 1998). The lake surface area is 0.4 km^2 and the catchment covers 2.37 km^2, which is mainly composed of K-alkaline phonotephrites and tephrifoidites (Hieke Merlin, 1967). The maximum depth is of 36 m on the northern part of the basin, but two thirds of the lake is less than 12 m deep. The maximum elevation in the catchment is 956 m a.s.l., with a maximum relief of 300 m. MON is considered a closed lake since no major in- or outflows exist. The trophic state of the present lake is eutrophic to hypertrophic. The climate at MON is characterized by wet winters and pronounced dry summers (Watts, 1996). Most of the annual precipitation (63 % of 815 mm mean annual precipitation) falls between October and March.

The geographical location of MON is in a favourable downwind position to the active volcanoes of the alkaline Roman Co-magmatic Province, as well as it is close by to the active volcanic centres of the Aeolian Islands (280 km), Mount Etna (360 km) and the Island of Pantelleria in the Strait of Sicily (540 km). Some of these eruptions were highly explosive in the past, and the erupted tephra material was widely dispersed in the Central Mediterranean and also deposited in the MON sediments (Narcisi, 1996; Wulf et al., 2004).

CPD
10, 2595–2626, 2014

3 Material and methods

Three long sediment cores used for this study were collected from Lago Grande di Monticchio at 13.5 m of water depth using the USINGER piston corer during different coring campaigns in 1994 and 2000. Core J (1994) is 65 m long and shows a continuous sequence of laminated sediments. Cores M/O (2000) were taken nearby and extend the laminated record to a length of 102.3 m (Brauer et al., 2007; Fig. 1). Sediment cores were split, imaged, described and correlated using macro- and microscopic marker tephras (Brauer et al., 2007). 32 m of the composite profile from cores M/O (67.45–74.67 m) and core J (40.92–64.98 m) were re-analysed for this study including varve counting, varve thickness measurements and micro-facies analyses. Microscopic analyses were carried out on a complete series of two-cm overlapping thin sections using a petrographic microscope under parallel and polarized light. Thin sections (100 mm × 20 mm) were prepared following the procedures described by Brauer et al. (2000). Varve counting was carried out applying two approaches: (method 1) overview counting of number of varves per cm at low microscopic magnification (50 ×), (method 2) counting based on thickness measurements for each varve at higher microscopic magnification (100 ×). Method 2 is regarded as more precise and has been applied for the first time for the MON sediments in this study. Varve counts obtained through method 2 were compared with a previous counting (method 1) performed by two different counters (Allen et al., 1999; Brauer et al., 2000, 2007). Elemental composition of the sediments was measured using an ITRAX µ-X-ray fluorescence (XRF) core scanner directly on the sediment cores with a step size of 300 µm resolution using a Cr-tube, 30 kV tube voltage, a tube current of 30 mA and 10 s exposure time. µ-XRF results are expressed as element intensities in counts. The high-resolution measurements provide 1–15 data points per varve depending on the annual sedimentation rate. 1354 marker layers were used to transfer the µ-XRF data on time scale using the varve counting-based age-depth model performed for the sedimentary record.

CPD
10, 2595–2626, 2014

4 Results

4.1 Varve counting and tephrochronology

The published varve chronology of the MON sediments (Brauer et al., 2007) is an independent chronology based on (1) varve counting (method 1) in sections where annual laminations have been recognised, and (2) a detailed calculation of sedimentation rates in sections where varves were poorly or not preserved using varve thickness measurements from adjacent varved sections. Tephra and turbidite layers were excluded from counting as non-annual events. The counting was from top to bottom, i.e., from young to old, and the whole chronology was established in two phases of counting: (1) from the present day back to 102 ka (MON-99), the chronology was developed by varve counting on the composite profile B/D and core J (Allen et al., 1999); and (2) extended by varve counting on the composite profile M/O for the interval 102 to 133 ka and a revision of the interval between 19.3 and 36.8 ka (MON-07; Brauer et al., 2007). The mean estimated accumulative varve counting error is ±5 % and varve chronology is supported by $^{40}Ar/^{39}Ar$ dates of major tephras and tephrochronology (Fig. 2a; Wulf et al., 2012). Since the MON-07 chronology is based on combination of varve counting, varve interpolation and tephra ages, absolute ages are expressed as "a".

For the present study, the MON-07 chronology has been re-examined by performing detailed varve counting (method 2) on a new composite profile J/M/O for the interval 76–112 ka (MON-2014). Thereby, three previously unidentified missing varve intervals have been noticed in core J within the interval 102.5–90.5 ka, which are now bridged by additional varve counts in the composite M/O. Based on these counts, a total of 510 additional varves have been counted and included in the new MON-2014 chronology. For most intervals the revised chronology (MON-2014) is in very good agreement with the MON-07 chronology (r = 0.999, Fig. 2b). MON-2014 is anchored to MON-07 chronology at the tephra layer TM 20–8 located on the top of the study interval and dated at 76 468 ± 3823 a (5 % accumulative counting error) (Wulf et al., 2012). The age-depth model along the study interval exhibits large changes in the sedimenta-

CPD
10, 2595–2626, 2014

tion rate (Fig. 2c), which is partly explained by the deposition of up to several meters thick tephra layers. In order to assess the uncertainties in the varve counts, the ages of five reliably correlated and well-dated tephra layers (Wulf et al., 2004, 2012) have been compared to the MON-2014 varve timescale (Fig. 2d). These tephras are (1) TM-21 (Petrazza Tuffs/Stromboli, 75.3 ± 6 ka K Ar^{-1}; Gillot and Keller, 1993), (2) TM-22 (Ignimbrite Z/Pantelleria, 86 ± 1.9 ka ^{40}Ar/^{39}Ar; Rotolo et al., 2013), (3) TM-23-11 (POP-1 tephra/Campanian Province, 92.4 ± 4.6 ka ^{40}Ar/^{39}Ar; Giaccio et al., 2012), (4) TM-25 (X-5 tephra/Campanian Province, 106.2 ± 1.3 ka ^{40}Ar/^{39}Ar; Giaccio et al., 2012) and (5) TM-27 (X-6 tephra/Campanian Province, 108.9 ± 1.8 ka ^{40}Ar/^{39}Ar; Iorio et al., 2014). The varve ages of tephras TM-27 (109.4 ka) and TM-25 (106.7 ka) are in good agreement with the age of the correlative tephras X5 and X6, but the varve chronology provides older ages for the tephras TM-23-11 (96.2 ka), TM-22 (89.4 ka) and TM-21 (78.6 ka) by ~ 3500 yr (Fig. 2c). Comparison between varve- and tephra dating agree each other on absolute ages for the period 110–106 ka with differences less than 0.5 %, but up to 4 % differences for the period 96–78 ka which, however, is still within the given dating uncertainties (Wulf et al., 2012). If the observed increasing difference between varve and tephra ages between 106 and 96 ka is real and caused by varve counting, we must assume either a varve underestimation or a sediment hiatus in this interval. However, we do not find any sedimentological indication for a hiatus and double varve counting in the J and M/O profiles always revealed about the same number of varves.

4.2 Microfacies analyses

The study interval covers the transition from last interglacial to glacial deposits (76–112 ka) in the MON record and is represented by a 31.12 m long interval predominantly consisting of finely organic varved sediments intercalated with intervals of more clastic varved sediments. Cm- to mm-thick deposits of reworked littoral sediments (minerogenic and organic detritus and tephra material) and 136 primary tephra fallout layers are randomly stratified in the laminated sequence. Varves are heterogeneous and seasonality is expressed by two or more of the following sub-layers: (i) a minerogenic

CPD
10, 2595–2626, 2014

detritus layer likely deposited during the winter season; (ii) a diatom layer as a result of the spring-summer peak of productivity in the lake and (iii) an authigenic siderite layer formed in autumn. Occasionally, endogenic calcite precipitation occurs in an additional late-spring/early-summer sub-layer (Fig. 3a and b).

On the basis of varve composition, two major micro-facies types distinguish organic varves (microfacies 1) form siderite varves (microfacies 2) and classified in two sub-types based on varve thickness and clastic content (sub-type a and b). The differentiation between both sub-types is made at an empiric value of 0.2 mm (mean plus standard error). Varve thickness variability is mainly controlled by the thickness of the winter sub-layer.

Microfacies 1a: Organic-diatomaceous varves with an average thickness of 0.15 mm (111 015–110 430; 108 630–105 500; 101 005–97 960; 96 760–94 250; 93 260–92 350; 88 905–85 780; 84 670–83 120; 81 440–79 305; 76 715–76 470 a). The varve structure is composed of two sub-layers: an organic detritus layer with high organic material content; and another one of diatoms. Varve thickness ranges from 0.1 to 1.8 mm.

Microfacies 1b: Organic-clastic-diatomaceous varves with an average thickness of 0.5 mm (92 070–88 905; 79 305–76 715 a). Varve structure is similar to microfacies 1a but the clastic content within the detritus sub-layer is higher. Endogenic carbonate precipitation (calcite or siderite) occasionally occurs in seasonal sub-layers. Varve thickness varies between 0.4 and 2.5 mm. The higher varve thickness compared with microfacies 1a is mainly due to higher clastic content in the winter sub-layer (Fig. 3b).

Microfacies 2a: Siderite-diatomaceous varves with an average thickness of 0.17 mm (103 000–101 000; 97 960–96 760; 94 250–93 260; 92 350–92 070; 85 780–84 670 a). These varves are composed of three laminae: clastic detritus, diatoms frustules and authigenic siderite. Varve thickness varies between 0.3 and 2.6 mm.

Microfacies 2b: Siderite-clastic-diatomaceous varves with an average thickness of 0.53 mm (111 230–111 015; 110 430–108 630; 105 500–103 000; 83 120–81 440 a). The varve structure is similar to microfacies 2a but the clastic content within the detritus sub-layer is higher. Varve thickness varies between 0.5 and 6 mm.

CPD
10, 2595–2626, 2014

The distribution of the microfacies within the stratigraphic sediment column distinguishes seven stratigraphic units and shows alternations between periods of thinner and thicker varves. Unit 1 (111.2–108.6 ka), unit 3 (92.1–88.9 ka), unit 5 (83.1–81.4 ka) and unit 7 (79.3–76.7 ka) are characterized by deposition of microfacies type b (thicker varves) and higher varve thickness variability (0.3–3 mm). In contrast, in unit 2 (108.6–92.1 ka), unit 4 (88.9–83.1 ka) and unit 6 (81.4–79.3 ka) microfacies type a (thinner varves) and lower inter-annual fluctuation prevail (Fig. 3c) with the exception of the interval 105.5–103 ka (microfacies 2b) within unit 2, which shows lightly thicker than average. Additionally, reworked deposits are thicker (> 0.5 mm) in unit 1, 3, 5 and 7 showing an additional detrital input from the catchment during the interval of thicker varves (Fig. 3c).

4.3 Element scanning

The heterogeneous nature of the MON sediments, i.e, organic-clastic-diatomaceous-siderite varves, reworked tephra material and primary tephra fallout layers, suggests multiple factors controlling the chemical element distribution. Microfacies analyses reveal changes in the clastic input are the major cause for varve thickness variability in the sediments. Hence, the terrigenous component of the sediments should allow the identification of different environmental processes controlling winter detrital influx into the lake. The lake catchment is composed of volcanic rocks rich in K-feldspar, foids, Fe-Ti-oxides and other mafic minerals such as pyroxenes, biotites and amphiboles (Zolitschka and Negendank, 1996). Measured element intensities of the Al are very low in comparison with other terrigenous elements such as the Ti, K and Fe, but its variability is closely related to the Ti along the whole sequence (Fig. 4a). The Ti–K scatter plot suggests two different K sources (Fig. 4b): K is proportional to Ti variability for values between 0 and 20 000 counts, but show independent behaviour for higher K-counts. A similar pattern is found for the Ti and the Fe (Fig. 4c). In contrast, the Ti and the Si are only weakly related suggesting different environmental indicators (Fig. 4d).

CPD
10, 2595–2626, 2014

Figure 3c shows some selected elements plotted against time together with complementary sedimentological information. Variability of Ti is associated with changes in varve thickness and composition at millennial timescales. Higher Ti-counts occur within thicker varves and clastic intervals (microfacies type b), while low values correspond to thinner organic varves (microfacies type a). Additionally, Ti variability resembles annual fluctuations in varve thickness within microfacies type b suggesting Ti-counts are controlled by winter detrital input into the lake. In contrast, the variability of K is much higher along the entire study interval and does not keep any clear relation with microfacies, varve thickness, reworked deposits or primary tephra layers. K/Ti ratios have been plotted in order to distinguish different K resources. This ratio is well correlated with primary tephra deposition, suggesting that higher K concentrations in the sediments (> 20 000 counts) correspond to volcanic ash (mainly of K-alkaline composition; Wutke et al., 2014) (Fig. 3c). Fe/Ti ratios show the Fe is associated with both siderite varves (microfacies 2) and tephra layers (Fig. 3c). The Si/Ti ratio (not shown) was calculated in order to distinguish biogenic silica and siliciclastic detrital matter. Higher values occur during the interval 100–92 ka and 88–76 ka, but this trend does not keep a clear relationship with increasing diatom sub-layer or with reworked deposits. Due to the ambiguous data we avoid using Si as an environmental or climate proxy in this study.

5 The Monticchio proxy data record

The palynological zonation defined in central Europe during the early Weichselian (Woillard, 1978) has been also identified in the MON pollen record (decadal resolution) (Fig. 3c). The stadial intervals Melisey 1 and 2 and Montaigu events, as well as the shorter cold oscillation termed Woillard event are reflected by sharp decreases of temperate Mediterranean woody taxa, which become replaced by non-arboreal pollen. Slightly increasing *Betula* pollen suggests cool and relatively humid conditions during these intervals in the Central Mediterranean region (Allen et al., 1999; Brauer et al.,

CPD
10, 2595–2626, 2014

2007). In contrast, the warm St. Germain 1and 2 interstadials are dominated in the MON record by mesic woody taxa similar to that during the Holocene (Brauer et al., 2007) (Fig. 3c). Complementary varve microfacies and varve thickness as well as high-resolution element scanning provide clues for a more comprehensive deciphering of environmental and climate changes at annual resolution (Fig. 3c). As mentioned above, varve thickness is mainly controlled by the thickness of the winter sub-layer (Fig. 3b) and closely related to the clastic influx into the lake as indicated by Ti-counts (Fig. 3c). Enhanced detrital matter flux is interpreted as a result of increased catchment erosion likely in response to changes in both precipitation and vegetation cover. Hence, varve thickness is applied as an integrating proxy for precipitation and temperature-driven vegetation changes. In addition, periods of thicker varves and higher detrital matter contents are characterized by a higher number of discrete turbidites reflecting an increased frequency of extreme events (Fig. 3c). Microfacies analyses reveals that slight increases in the thickness of diatom sub-layer are related to thicker detrital sub-layers (Fig. 3b), probably because of higher external nutrient input into the lake during the winter season. A bias of varve thickness by reworked tephra after deposition of thick tephra layers might be only a minor effect since no relationship between thicker tephra deposits and subsequent increase in varve thickness has been observed (Fig. 3c). This can be demonstrated, for example, for TM-25, one of the thickest tephra layers in MON. Despite increased K-counts in the ca. 250 varves following the ash deposit indicating some tephra material reworking, there is no significant increase in varve thickness observed (Fig. 3c).

Based on varve microfacies analyses and Ti-counts as proxy for detrital matter flux, a succession of six periods of increased clastic input (microfacies type b) interpreted as cold and wet intervals occurred during the studied time sequence and labeled as MON 1–6 (Fig. 3c, Table 1). Four of these intervals coincide with the pollen zones Melisey 1 and 2 and the pollen-defined Woillard and Montaigu oscillations (Brauer et al., 2007). Based on the new high-resolution varve data we are now able to define the boundaries of these climatic oscillation more precisely than with the lower resolution

CPD
10, 2595–2626, 2014

pollen data alone. In the following we describe the succession of cold and wet climate intervals in more detail and in stratigraphical order.

MON 1 (111.2–111 ka) lasted 217 varve yr and the onset and the end of this climatic oscillation occurred within a year (Table 1). MON 1 corresponds to Woillard event, which is reflected by five pollen samples indicating vegetation changes within less than 50 yr (the limit of pollen data resolution). The duration of MON 1 as given here is about 100 yr shorter than the previously published duration of Woillard event as defined by pollen data (Brauer et al., 2007). This is mainly due to the fact that boundaries of this short climatic oscillation could not be precisely captured because of the insufficient resolution of the pollen data. In addition to the less precise boundary definition in the lower resolution pollen data, part of the different durations of MON 1 (this study) and the Woillard (Brauer et al., 2007) can be explained by 15 more varves counted in the MON-07 chronology compared to the MON-2014 time scale.

MON 2 (110.4–108.6 ka) occurred only ca. 600 yr after MON 1 but lasted much longer (1798 varves yr). The transitions in the varve data are very sharp and comprise only 7 varves at the onset and 20 varves at the end. However, the pollen boundaries of the corresponding Melisey 1 stadial are sharp only at the onset (ca. 40 varves – i.e., limit of sample resolution), whereas the end occurred gradually over ca. 800 varve yr. Since the upper (biostratigraphic) boundary of Melisey (Brauer et al., 2007) has been defined at the onset of the gradual decrease this period is not included in Melisey 1. Therefore, the duration of MON 2 (1798 varves in MON-2014 counts) and Melisey 1 (1900 varves in MON-07 counts) are similar.

The varve signal for MON 3 (105.5–103 ka) is less clear than for the other oscillations in the transitions are more gradual (Table 1; Fig. 3). Similarly, the decrease of arboreal pollen during the Montaigu is less pronounced and tree pollen percentages remain at ca. 70 % level, whereas within Melisey 1 and 2 tree pollen decreased down to ~ 20 % (Fig. 3c; Brauer et al., 2007). In addition, the transitions in and out of the Montaigu event appear very gradual with slight forest deterioration during the first 1100 varve yr of the oscillation and a subsequent recovery during the following 2500 varve yr

CPD
10, 2595–2626, 2014

(Brauer et al., 2007). In contrast, the onset of the varve-defined MON 3 interval is defined 1130 varve yr earlier because the increase of varve thickness and detrital matter flux responded with a time lag to the vegetation change only when mesic woody taxa already had reached lowest values in the about the middle of Montaigu event. For this reason the pollen defined Montaigu comprises 3600 varve yr compared to the shorter varve-defined MON 3 (2500 varve yr; Fig. 3c). Interestingly, the recovery of tree pollen at the end of the Montaigu event occurred synchronously with varve changes at the end of MON 3.

MON 4 (92.1–88.9 ka) began ca. 10 900 varve yr after the end of MON 3 and started and ended abruptly within a decade. The first phase of MON 4 is characterized by two peaks in varve thickness interrupted by a short interval of thin varves (180 varve yr). The transitions in the corresponding pollen zone Melisey 2 appear slightly more gradual because of the lower sample resolution of ca. 80 varve. The durations of MON 4 (3162 varve yr) differs from the length of Melisey 2 (2670 varve yr) estimated by the MON-2007 chronology (Brauer et al., 2007) because 510 additional varves have been counted in the revised MON-2014 varve counting within the interval between ca. 102.5 and 90.5 ka (see Sect. 4.1). So, the duration of the thicker varve interval MON 4 and the pollen interval Melisey 2 are in a good agreement.

The two youngest thick varve intervals MON 5 (83.1–81.4 ka) and MON 6 (79.3–78.3 ka) correspond to periods of decreasing tree pollen and increasing non-arboreal pollen labelled as PAZ 17d and 17b by Allen et al. (1999). MON 5 started abruptly but the maximum in varve thickness only occurred in the middle of this interval coinciding with the lowest values of mesic woody taxa. While pollen data suggest gradual forest deterioration at the onset, the end of this climate oscillation is abrupt in both the pollen and the varve thickness records (Fig. 3c). The duration of this interval as defined by varve data is 1681 varve yr (Table 1). MON 6 is located at the top of the studied interval and comprises two centennial-scale oscillations with the first one lasting ca. 400 varve yr coinciding with a rapid decrease in arboreal pollen from 80 to 20 %. About 1000 varve yr later tree pollen recovered to ca. 40 % coinciding with a decrease

CPD
10, 2595–2626, 2014

in varve thickness and Ti-counts. The second fluctuation lasted ca. 300 varve yr ca. 1000 varve yr lafter the first one. This interval is marked by an abrupt increase in Ti-counts and varve thickness, as well as a reduction in tree pollen to 35 %. The following recovery of tree vegetation after MON 6 did not reach values above 45 %, suggesting a major shift of the environment from an interglacial to the glacial mode (MIS 5a/4 transition).

In summary, changes in vegetation coincide within the limit of pollen data resolution with those five oscillations that are characterised by rapid transitions and distinct proxy responses MON 1 and 2 and MON 4 to 6. Only for the MON 3 oscillation the varve response lagged the vegetation changes at the beginning of the Montaigu event. Interestingly, both the MON 3 and the Montaigu event exhibit the lowest amplitutes of proxy changes of all investigated oscillations and, in addition, are characterized by gradual transition wheres all other oscillations befan and ended abruptly.

The strongest signals in pollen data (i.e. reduction of tree pollen) are observed for the younger cold intervals (Melisey 2, PAZ 17d, PAZ 17b) occurring after ca. 92 ka, whereas the most pronounced varve changes occur for the earliest cold oscillations MON 1 and MON 2 at the end of the last interglacial, as well as for MON 4. Hence, the longest cold oscillation MON 4/Melisey 2 (3162 varve yr) is the only interval with a strong signal observed in both data sets.

6 Comparison to the NGRIP and NALPS isotope records

6.1 Duration of the cold spells along a transect from Greenland to the Mediterranean

The new annual sedimentological data in combination with the previously published pollen record and the independently established chronology allows detailed high-resolution comparison of the MON (40° N) sediment record along a NW–SE transect across western Europe including the high resolution δ^{18}O NALPS stalagmite (Boch

CPD
10, 2595–2626, 2014

et al., 2011) from the Austrian Alps (47° N) and NGRIP ice core (75° N) in order to investigate similarities and differences between these key climate archives (Fig. 5). For the NGRIP record we show both the updated GICC05modelext (Wolff et al., 2010) and the new AICC2012 timescales (Bazin et al., 2013; Veres et al., 2013). Our comparisons are solely based on visual inspections of major changes in the proxy data and are based on independently established chronologies with their inherent uncertainties. We explicitly avoid any kind of wiggle matching of climate proxy data and re-interpretation of published chronologies. Although the overarching goal of such comparison is to decipher leads and lags in regional climate change we are aware that the chronological uncertainties hamper this approach. In addition, it must be taken into consideration that the sediment proxies may not respond in the same way to climate change than stable isotopes in stalagmites and ice cores. Nevertheless, the high-resolution data allows a very detailed view from different regional and proxy perspectives particularly on the succession and evolution of cold climatic fluctuations that occurred during the approximately 35 kyr long period between full interglacial and a full glacial mode. In order to circumvent problems due to discrepancies in absolute ages we first compare the duration of the identified cold oscillations as well as the amplitudes and structure of proxy changes.

The first cold oscillation in the MON record (MON 1) occurred after several millennia of rather stable interglacial climate and was the shortest and lasted only 217 (Table 1). MON 1 corresponds to the Woillard event defined in the Grande Pile pollen stratigraphy in the French Vosges mountains (Woillard, 1978). Interestingly, this cooling episode does not appear as a discrete fluctuation in NGRIP (Capron et al., 2010), but likely corresponds to the end of the stepwise isotope change during the final phase of GI 25. The short warming at the very end of GI 25 also known as "GI 25 rebound" might be reflected in the MON record as the 600 yr long thinner varve interval between MON 1 and MON 2 (Fig. 5). The NALPS record exhibits an interruption of speleothem growth at the end of the interglacial so that a comparison with MON 1 is not possible. MON 1 is assumed to further correlate with the North Atlantic cold event C25 at the MIS 5e/d

CPD
10, 2595–2626, 2014

transition (Chapman and Shackleton, 1999). Both MON 1 and C25 marked the onset of the recurrent rapid cold spells during MIS 5d-a after stable MIS 5e conditions (Chapman and Shackleton, 1999).

The second cold spell MON 2 (Melisey 1) is assumed to correlate with GS25. It is a very distinct oscillation in both the MON and the NGRIP record but only partly recorded in NALPS because of a hiatus (Boch et al., 2011). One could imagine that the cessation of stalagmite growth during the first phase of this cold spell was the response to this cooling. The length of MON 2 (ca. 1800 yr) resembles better the duration of GS 25 on the AICC2012 time scale (1990 yr) than on the GICC05 chronology (2360 yr).

The third cold spell in the MON record (MON 3) broadly correlates to GS 24 in NGRIP and in NALPS. However, the weak signal and gradual transitions in the MON proxies and the differences between pollen and sediment signals make it difficult to define sharp and unequivocal boundaries for this oscillation in the MON record. The longer duration of MON 3 (2500 yrs) compared to GS 24 in AICC2012 (950 yrs); Veres et al., 2013), GICC05 (920 yrs; Wolff et al., 2010) and NALPS (1040 ± 585 yrs; Boch et al., 2011) (Table 2) can be explained by differences in boundary definition and, more specifically, by the occurrence of several short-lived variations in varve thickness which are included in MON 3 (Fig. 5). These fluctuations seem to resemble the short warming (precursor GI 23) and subsequent cooling events preceding GI 23 in the NGRIP and NALPS records (Fig. 5), which, however, there are not included in the duration of GS 24 (Capron et al., 2010; Boch et al., 2011).

MON 4 (Melisey 2) correlates with GS 22. The duration of GS 22 is still under discussion and varies in different ice core chronologies between 2480 yrs (GICC05), 2620 yrs (revised GICC05 timescale; Vallelonga et al., 2012) and 2760 yrs (AICC2012; Veres et al., 2013). All ages suggest a shorter duration than determined in the NALPS record (3250 yrs), which in turn is in good agreement with the Monticchio estimate of MON 4 (3171 ± 9 yrs; Table 2). Two phases of reduced varve thickness occurring during 500 yr after MON 4 (not included in MON 4) might correlate with two short-lived warming events (precursor GI 21 I and II) at the onset of GI 21 (Boch et al., 2011) (Fig. 5).

CPD
10, 2595–2626, 2014

MON 5 and 6 are assumed to correlate with GS21 and GS20, respectively. The length of MON 5 (1680 yrs) is in very good agreement with the duration of GS 21 in NALPS (1720 yrs) but ca. 350 yrs longer than determined by the ice core chronology (Table 2). Similarly, MON 6 (2590 yrs), also is 340 yr longer than GS 20 in Greenland. In the NALPS record a cold phase correlating with MON 6 is not recorded due to growth cessation of the stalagmites.

6.2 Absolute dating implications

Millennial-scale climatic fluctuations identified in the MON varved record are in broad agreement with Alpine stalagmites and Greenland ice cores, although absolute dating still reveals differences. The MON-2014 chronology is in good agreement for the three older oscillations MON 1 to MON 3 occurring before 100 ka, while the AICC2012 timescale reveals younger ages for this interval mainly because of a shorter duration estimated for the GI 23–GI 22 interstadial. For the younger oscillations (MON 4 to MON 6) occurring after 100 ka the ice core and NALPS chronologies show quite good agreement, while the Monticchio chronology suggests consistently 3500 yrs older ages. This difference is caused by the shorter duration revealed for the interstadial interval between MON 3 and MON 4 (9500 yrs) compared to the durations determined for the corresponding GI 23–GI 22 period in Greenland (14 000 yrs in GICC05; 12 500 in AICC2012; Table 3). Therefore, we must assume a so far undiscovered bias of the varve chronology during this time interval although no conspicuous indications have been found in the sediment sequence. A possible problem in this part of the varve chronology is further suggested by the kink in the sedimentation rate curve and the discrepancy between the varve ages and tephra ages between ca. 106 and 96 ka shown in Fig. 2c and d (see Sect. 4.1).

CPD
10, 2595–2626, 2014

7 Conclusions

Intervals of thicker varves and high Ti counts identified in the sediment record of Lago Grande di Monticchio resemble both millennial- and sub-millennial scale abrupt climatic changes during the early stage of the last glaciation. Six major oscillations in varve sedimentation (MON 1–6) can be identified between 76 and 112 ka, which coincide with cool and humid episodes as derived from the Monticchio pollen record. The annual resolution of the sediment proxies allows (i) a more precise definition of these cold intervals, and (ii) deciphering the velocity of change at the transitions. This new dataset also provides the opportunity to precisely compare, the Mediterranean response to abrupt climate changes with those recorded in Greenland and northern Alps. The oscillations MON 2–6 are assumed to correlate with GS 25–20, respectively. Despite still existing uncertainties in the absolute dating of these oscillations especially between 100 and 76 ka we can discuss similarities and differences in amplitude of proxy responses and the durations of the climatic oscillations:

- MON 1, the first clear signal of cooling seen in the Mediterranean, has no counterpart in the NGRIP record but coincides with the lowest values at the end of the stepwise isotope change during the second half of GI 25.
- MON 2 (GS25) and MON 4 (GS22) were the longest millennial-scale cold intervals in all records with durations between 1850 and 2360 yr (MON 2, GS25) and between 2620 and 3250 yrs (MON 4, GS22).
- The largest difference between the Monticchio varve data and Greenland and speleothem isotopes is observed for MON 3, which shows the least pronounced sediment changes of all Monticchio oscillations and is characterised by gradual transitions. The corresponding GS 24 in NGRIP also is the least pronounced stadial in the studied time interval, although still more distinct than MON 3. The corresponding oscillation in the NALPS record, however, is very strong and shows a ca. 2 ‰ decrease in $\delta^{18}O$. Explanations for the attenuated response to the

CPD
10, 2595–2626, 2014

climate change in the Mediterranean at that time remain elusive so far, but, interestingly, this cold interval occurred during a period of lower global ice volume (MIS 5c).

– The coldest episodes in Greenland were GS 21 and GS 20, which already reached glacial isotope values (ca. −44 ‰). Excluding GS 24, there is a general increasing trend in the amplitude of the stadials in NGRIP from GS 25 to 20. A similar trend is seen in the MON pollen record but not as distinct as in the ice core. The growth cessation of the stalagmites in the northern Alps during GS 21 and GS 20 might also support cooler stadials at the end of the MIS 5. In contrast, in the Monticchio record the most pronounced cold spells are MON 2 and MON 4, suggesting larger environmental impacts in the Mediterranean coinciding with the stages of higher global ice volume MIS 5d and MIS 5b, respectively.

Millennial-scale cold climatic oscillations occurring during the early phase of the last glaciation are in brad agreement between the Greenland the Alps and the central Mediterranean. However, a more detailed look revealed certain differences between the the Greenland and NALPS isotope records and the varve and pollen record from Monticchio. These differences might be an expression of (i) different amplitudes of climate change, (ii) different proxy responses, and (iii) dating uncertainties. Further investigations are needed to better disentangle these factors to better assess regional aspects of past climate change.

Acknowledgements. We thank D. Berger, M. Köhler, M. Prena, R. Scheuss, S. Opitz and D. Axel for the retrieval of sediment cores during the coring campaign in 2000. Special thanks are due to G. Arnold, M. Köhler and D. Berger for thin section preparation, A. Hendrich for graphical support and Jens Mingram and Christoph Spötl for comments and suggestions on a previous version of the manuscript. This study was funded by the GFZ German Research Centre for Geosciences, Potsdam, Germany, and is a contribution to the Helmholtz-Association climate initiative REKLIM (Topic 8 “Rapid Climate Change from Proxy data”).

CPD
10, 2595–2626, 2014

The service charges for this open access publication have been covered by a Research Centre of the Helmholtz Association.

References

Allen, J. R. M., Brandt, U., Brauer, A., Hubberten, H., Huntley, B., Kraml, M., Mackensen, A., Mingram, J., Negendank, È. F. W., Nowaczyk, N. R., Watts, W. A., Wulf, S., and Zolitschka, B.: Rapid environmental changes in southern Europe during the last glacial period, Nature, 400, 740–743, 1999.

Andersen, K. K., Azuma, N., Barnola, J.-M., Bigler, M., Biscaye P., Caillon, N., Chappellaz, J., Clausen H. B., Dahl-Jensen, D., Fischer, H., Flückiger, J., Fritzsche, D., Fujii, Y., Goto-Azuma, K., Grønvold, K., Gundestrup, N. S., Hansson, M., Huber, C., Hvidberg, C. S., Johnsen, S. J., Jonsell, U., Jouzel, J., Kipfstuhl, S., Landais, A., Leuenberger, M., Lorrain, R., Masson-Delmotte, V., Miller, H., Motoyama, H., Narita, H., Popp, T., Rasmussen, S. O., Raynaud, D., Rothlisberger, R., Ruth, U., Samyn, D., Schwander, J., Shoji, H., Siggard-Andersen, M.-L., Steffensen, J. P., Stocker, T., Sveinbjörnsdóttir, A. E., Svensson, A., Takata, M., Tison, J.-L., Thorsteinsson, Th., Watanabe, O., Wilhelms, F. and White, J. W. C.: High-resolution record of Northern Hemisphere climate extending into the last interglacial period, Narue, 431, 147–151, 2004.

Bazin, L., Landais, A., Lemieux-Dudon, B., Toyé Mahamadou Kele, H., Veres, D., Parrenin, F., Martinerie, P., Ritz, C., Capron, E., Lipenkov, V., Loutre, M.-F., Raynaud, D., Vinther, B., Svensson, A., Rasmussen, S. O., Severi, M., Blunier, T., Leuenberger, M., Fischer, H., Masson-Delmotte, V., Chappellaz, J., and Wolff, E.: An optimized multi-proxy, multi-site Antarctic ice and gas orbital chronology (AICC2012): 120–800 ka, Clim. Past, 9, 1715–1731, doi:10.5194/cp-9-1715-2013, 2013.

Boch, R., Cheng, H., Spötl, C., Edwards, R. L., Wang, X., and Häuselmann, Ph.: NALPS: a precisely dated European climate record 120–60 ka, Clim. Past, 7, 1247–1259, doi:10.5194/cp-7-1247-2011, 2011.

Brauer, A., Mingram, J., Frank, U., Gu, C., Schettler, G., Wulf, S., Zolitschka, B., and Negendank, K. F. W.: Abrupt environmental oscillations during the Early Weichselian recorded at Lago Grande di Monticchio, southern Italy, Quaternary Int., 74, 79–90, 2000.

CPD
10, 2595–2626, 2014

Brauer, A., Allen, J. R. M., Mingram, J., Dulski, P., Wulf, S., and Huntley, B.: Evidence for last interglacial chronology and environmental change from Southern Europe, P. Natl. Acad. Sci. USA, 104, 450–455, 2007.
Brocchini, D., La Volpe, L., Laurenzi, M. A., and Principe, C.: Storia evolutiva del Monte Vulture, Plinius, 12, 22–25, 1994.
Capron, E., Landais, A., Chappellaz, J., Schilt, A., Buiron, D., Dahl-Jensen, D., Johnsen, S. J., Jouzel, J., Lemieux-Dudon, B., Loulergue, L., Leuenberger, M., Masson-Delmotte, V., Meyer, H., Oerter, H., and Stenni, B.: Millennial and sub-millennial scale climatic variations recorded in polar ice cores over the last glacial period, Clim. Past, 6, 345–365, doi:10.5194/cp-6-345-2010, 2010.
Chapman, M. R. and Shackleton, N. J.: Global ice-volume fluctuations, North Atlantic ice-rafting events, and deep-ocean circulation changes between 130 and 70 ka, Geology, 27, 795–798, 1999.
Drysdale, R. N., Zanchetta, G., Hellstrom, J. C., Fallick, A. E., McDonald, J., and Cartwright, I.: Stalagmite evidence for the precise timing of North Atlantic cold events during the early last glacial, Geology, 35, 77–80, 2007.
Giaccio, B., Nomade, S., Wulf, S., Isaia, R., Sottili, G., Cavuoto, G., Galli, P., Messina, P., Sposato, A., Sulpizio, R., and Zanchetta, G.: The late MIS 5 Mediterranean tephra markers: a reappraisal from peninsular Italy terrestrial records, Quaternary Sci. Rev., 56, 31–45, 2012.
Gillot, P.-Y. and Keller, J.: Radiochronological dating of Stromboli, Acta Vulcanologica 3, 69–77, 1993.
Harting, P.: De Bodem van Het Eemdal, Verslagen en Verhandelingen Koninklijke, Academie van Wetenschappen, 1874.
Hays, J. D., Imbrie, J., and Shackleton, N. J.: Variations in the Earth's Orbit: Pacemaker of the Ice Ages, Science, New York, 194, 1121–32, 1976.
Hieke Merlin, O.: I prodotti vulcanici del Monte Vulture, Memorie degli istituti di geologia e Mineralogia dell'Università di Padova XXVI, 1–65, 1967.
Iorio, M., Liddicoat, J., Budillon, F., Incoronato, A., Coe, R. S., Insinga, D. D., Cassata, W. S., Lubritto, C., Angelino, A., and Tamburrino, S.: Combined palaeomagnetic secular variation and petrophysical records to time-constrain geological and hazardous events: an example from the eastern Tyrrhenian Sea over the last 120 ka, Global Planet. Change, 113, 91–109, 2014.

CPD
10, 2595–2626, 2014

Kukla, G.: How long and how stable was the last interglacial? Quaternary Sci. Rev., 16, 605–612, 1997.

Kukla, G. J., Bender, M. L., de Beaulieu, J.-L., Bond, G., Broecker, W. S., Cleveringa, P., Gavin, J. E., Herbert, T. D., Imbrie, J., Jouzel, J., Keigwin, L. D., Knudsen, K.-L., McManus, J. F., Merkt, J., Muhs, D. R., Müller, H., Poore, R. Z., Porter, S. C., Seret, G., Shackleton, N. J., Turner, C., Tzedakis, P. C., and Winograd, I. J.: Last interglacial climates, Quaternary Res., 58, 2–13, 2002.

Landais, A., Barnola, J. M., Kawamura, K., Caillon, N., Delmotte, M., Van Ommen, T., Dreyfus, G., Jouzel, J., Masson-Delmotte, V., Minster, B., Freitag, J., Leuenberger, M., Schwander, J., Huber, C., Etheridge, D., and Morgan, V.: Firn-air δ^{15}N in modern polar sites and glacial–interglacial ice: a model-data mismatch during glacial periods in Antarctica?, Quaternary Sci. Rev., 25, 49–62, 2006.

Mangerud, J., Dokken, T., Hebbeln, D., Heggen, B., Ingolfsson, O., Landvik, J. Y., Mejdahl, V., Svendsen, J. I., and Vorren, T. O.: Fluctuations of the Svalbard–Barents Sea ice-sheet during the last 150 000 years, Quaternary Sci. Rev., 17, 11–42, 1998.

McManus, J. F., Bond, G. C., Broecker, W. S., Johnsen, S., Labeyrie, L., and Higgins, S.: High-resolution climate records from the North Atlantic during the last interglacial, Nature, 371, 326–329, 1994.

Narcisi, B.: Tephrochronology of a late quatternary lacustrine record from the monticchio maar (vulture volcano, southern Italy), Quaternary Sci. Rev., 15, 155–165, 1996.

Rahmstorf, S.: Ocean circulation and climate during the past 120 000 years, Nature, 419, 207–14, 2002.

Rotolo, S. G., Scaillet, S., La Felice, S., and Vita-Scaillet, G.: A revision of the structure and stratigraphy of pre-Green Tuff ignimbrites at Pantelleria (Strait of Sicily), J. Volcanol. Geoth. Res., 250, 61–74, 2013.

Sánchez Goñi, M. F., Eynaud, F., Turon, J. L., and Shackleton, N. J.: High resolution palynological record off the Iberian margin: direct land-sea correlation for the Last Interglacial complex, Earth Planet. Sc. Lett., 171, 123–137, 1999.

Shackleton, N. J.: Oxygen isotopes, ice volume and sea level, Quaternary Sci. Rev., 6, 183–190, 1987.

Shackleton, N. J., Chapman, M., Sánchez-Goñi, M. F., Pailler, D., and Lancelot, Y.: The classic marine isotope substage 5e, Quaternary Res., 58, 14–16, 2002.

CPD
10, 2595–2626, 2014

Stoppa, F. and Principe, C.: Erratum to "Eruption style and petrology of a new carbonatitic suite from the Mt. Vulture (Southern Italy): The Monticchio Lakes Formation" [Journal of Volcanology and Geothermal Research 78 (1997) 251–265], J. Volcanol. Geoth. Res., 80, 137–153, 1998.

Vallelonga, P., Bertagna, G., Blunier, T., Kjær, H. A., Popp, T. J., Rasmussen, S. O., Steffensen, J. P., Stowasser, C., Svensson, A. S., Warming, E., Winstrup, M., Bigler, M., and Kipfstuhl, S.: Duration of Greenland Stadial 22 and ice-gas Δage from counting of annual layers in Greenland NGRIP ice core, Clim. Past, 8, 1839–1847, doi:10.5194/cp-8-1839-2012, 2012.

Veres, D., Bazin, L., Landais, A., Toyé Mahamadou Kele, H., Lemieux-Dudon, B., Parrenin, F., Martinerie, P., Blayo, E., Blunier, T., Capron, E., Chappellaz, J., Rasmussen, S. O., Severi, M., Svensson, A., Vinther, B., and Wolff, E. W.: The Antarctic ice core chronology (AICC2012): an optimized multi-parameter and multi-site dating approach for the last 120 thousand years, Clim. Past, 9, 1733–1748, doi:10.5194/cp-9-1733-2013, 2013.

Watts, W.: Vegetation history and palaeoclimate of the last glacial period of Lago Grande di Monticchio, southern Italy, Quaternary Sci. Rev., 15, 133–153, 1996.

Woillard, G. M.: Grande Pile peat bog: a continuous pollen record for the last 140 000 years, Quaternary Res., 9, 1–21, 1978.

Wolff, E. W., Chappellaz, J., Blunier, T., Rasmussen, S. O., and Svensson, A.: Millennial-scale variability during the last glacial: The ice core record, Quaternary Sci. Rev., 29, 2828–2838, 2010.

Wright, J. D.: Quaternary Geochronology: Methods and Applications, American Geophysical Union, 2000.

Wulf, S., Kraml, M., Brauer, A., Keller, J., and Negendank, J. F. W.: Tephrochronology of the 100 ka lacustrine sediment record of Lago Grande di Monticchio (southern Italy), Quaternary Int., 122, 7–30, 2004.

Wulf, S., Keller, J., Paterne, M., Mingram, J., Lauterbach, S., Opitz, S., Sottili, G., Giaccio, B., Albert, P. G., Satow, C., Tomlinson, E. L., and Viccaro, M.: The 100 e 133 ka record of Italian explosive volcanism and revised tephrochronology of Lago Grande di Monticchio, Quaternary Sci. Rev., 58, 104–123, 2012.

Zolitschka, B. and Negendank, J. F. W.: Sedimentology, dating and palaeoclimatic interpretation of a 76.3 ka record from Lago Grande di Monticchio, southern Italy, Quaternary Sci. Rev., 15, 101–112, 1996.

CPD
10, 2595–2626, 2014

Table 1. Timing and duration of climatic oscillations MON 1–6 and their transitions (abruptness of varve thickness changes) onto the MON-2014 timescale. Correlative events in terrestrial, marine and ice core stratigraphies across from Greenland to the Mediterranean are given for comparison.

MON oscillations varve-defined	From (a)	Transition (varve yr)	To (a)	Transition (varve yr)	Duration (varve yr)	Pollen-defined intervals	North Atlantic correlates	Greenland correlates	MIS
MON 1	111 230	0	111 013	1	217	Woillard	C25		5d
MON 2	110 429	7	108 631	20	1798	Melisey 1	C24	GS 25	5d
MON 3	105 500	33	103 000	153	2500	Montiegu	C23	GS 24	5c
MON 4	92 069	11	88 907	11	3162	Melisey 2	C21	GS 22	5b
MON 5	83 121	3	81 440	7	1681	PAZ 17d		GS 21	5a
MON 6	79 307	3	76 715	13	2592	PAZ 17b		GS 20	5a

CPD
10, 2595–2626, 2014

Table 2. Duration of the millennial-scale climatic oscillations (stadial and interstadials) in the four different independent chronologies from Greenland to the Mediterranean. NGRIP $\delta^{18}O_{ice}$ as constrained on GICC05 chronology (Wolff et al., 2010) and AICC2012 timescale (Veres et al., 2013); NALPS composite speleothem $\delta^{18}O$ record (Boch et al., 2012); and MON varve thickness record (this study). The duration of the MON oscillations has been rounded.

Climatic oscillation	GICC05 (yr)	AICC2012 (yr)	NALPS (yr)	MON (varve yr)
GI20	2340	2166		2592
GS21 (MON 5)	1320	1340	1720	1681
GI21	7000	7009	7450	6455
GS22 (MON 4)	2620	2760	3250	3162
GI23 + GS23	14 000	12 512	–	10 930
GS24 (MON 3)	920	950	1040	2500*
GI24	2840	2650	3090	3130
GS25 (MON 2)	2360	1990		1798

CPD
10, 2595–2626, 2014

Table 3. Absolute dating of the millennial-scale climate transitions in the four different independent timescales from Greenland to the Mediterranean. NGRIP $\delta^{18}O_{ice}$ as constrained on GICC05 chronology (Wolff et al., 2010) and AICC2012 timescale (Veres et al., 2013); NALPS composite speleothem $\delta^{18}O$ record (Boch et al., 2012); and MON varve thickness record (this study).

Climatic oscillation	GICC05 (a)	AICC2012 (a)	NALPS (a)	MON (a)
GI19	72 090		71 690	78 300
GS20 (MON 6)	74 070	73 896		79 260
GI20	76 410	76 062	75 860	81 190
GS21 (MON 5)	77 795	77 402	77 580	82 455
GI21	84 730	84 411	85 030	88 905
GS22 (MON 4)	87 630	87 171	88 690	92 070
GI23	103 995	102 150	103 550	103 000
GS24 (MON 3)	105 410	103 100	105 210	105 500
GI24	108 250	105 750	108 300	108 630
GS25 (MON 2)	110 620	107 740		110 430

CPD
10, 2595–2626, 2014

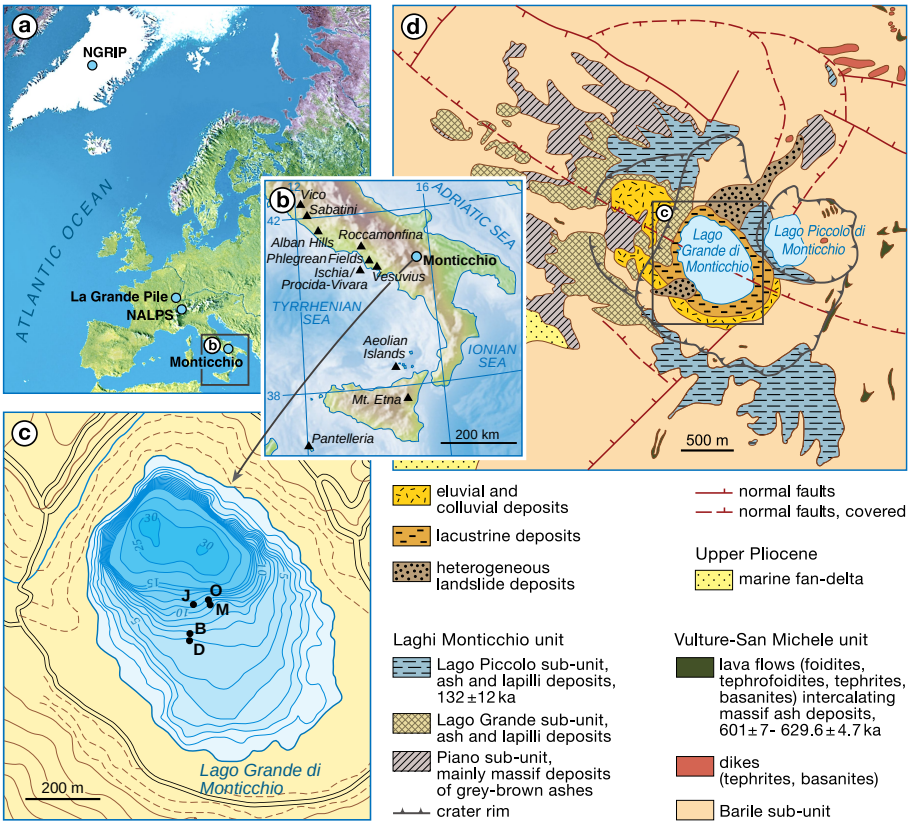

Figure 1. (a) Location of Lago Grande di Monticchio and the sites mentioned in the text and used for comparison. **(b)** Bathymetry of the lake and coring sites. **(c)** Geological map of the catchment of the lake.

CPD
10, 2595–2626, 2014

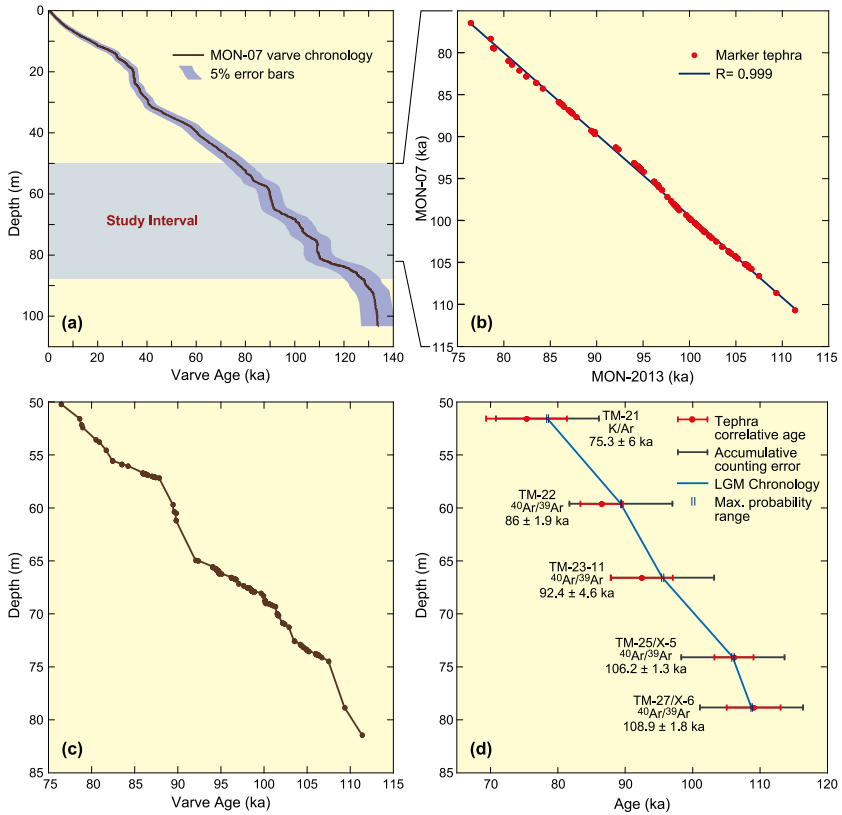

Figure 2. Varve chronology of the Lago Grande di Monticchio sedimentary record: **(a)** MON-07 age-depth model for the last 133 kyrs as derived from varve counting (Brauer et al., 2007). Error bars showing the 5 % error range. **(b)** comparison between MON-07 and MON-2014 varve counts for the study interval (76–112 ka); **(c)** MON-2014 age-depth model (this study); **(d)** comparison of the MON-2014 timescale and radiometric ages of tephra correlatives.

CPD
10, 2595–2626, 2014

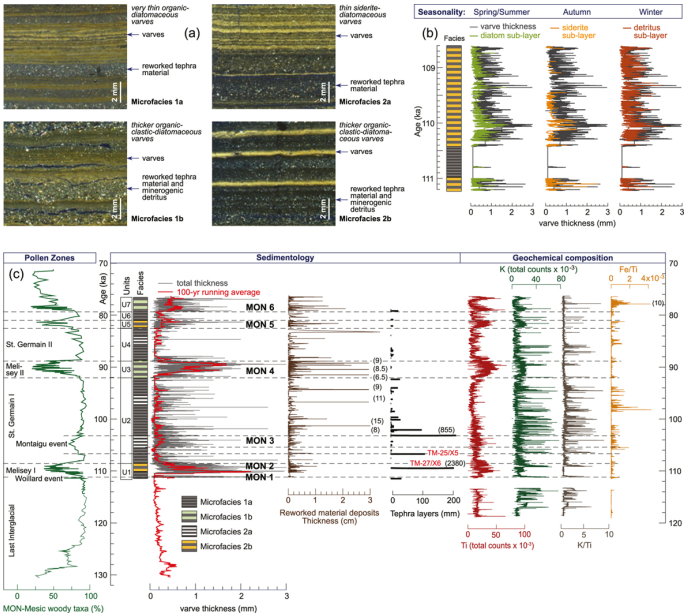

Figure 3. Sedimentological and elemental composition of the varved sediments of Lago Grande di Monticchio: **(a)** thin section images of the varved sediments of MON showing the different types of microfacies. **(b)** Schematic lithological profile from 111 to 108 ka (microfacies 1a and 2b); total varve thickness (grey) compared with thickness variability of the different sub-layers; **(c)** environmental and climate proxies, from left to right: mesic woody taxa percentages (decadal resolution) on MON-2014 timescales (modified from Brauer et al., 2007) and pollen sub-zones; schematic lithological profile of the study interval; varve thickness variability (grey line) and 100 yr average sedimentation rate (red line; data for the interval 112–133 ka have been taken from Brauer et al., 2007); thickness variability reworked material deposits; thickness of the primary tephra layers; distribution of the Ti and K as derived from µXRF measurements and the K/Ti and Fe/Ti ratios throughout the sediment record.

CPD
10, 2595–2626, 2014

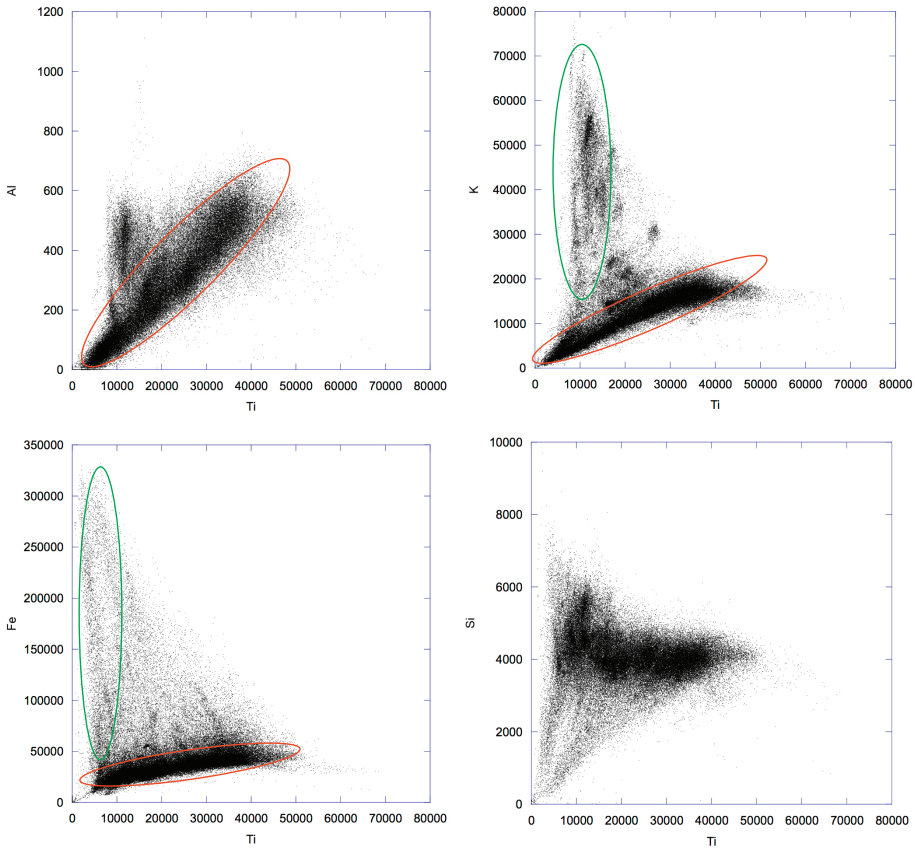

Figure 4. Scatter plots for major terrigenous elements as derived from µXRF measurements.

CPD
10, 2595–2626, 2014

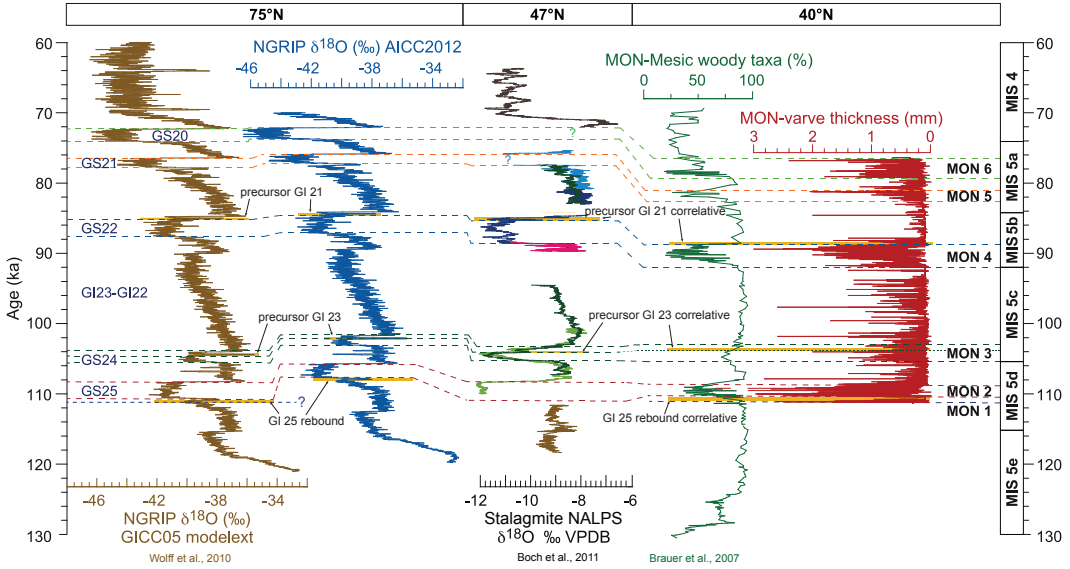

Figure 5. MON varve thickness and pollen record compared to the NGRIP ice core δ^{18}O record in both GICC05 and AICC2012 timescales, NALPS record, covering a NW–SE transect from 75° N to 40° N in western Europe. Marine isotope 5 sub-stages (MIS) start dates according to Wright, 2000 and Greenland stadials (GS) identified in the NGRIP and NALP δ^{18}O records are shown for comparison. Dashed lines indicate the boundaries of the MON oscillations and their correlatives GS. Duration of the GS is derived from Veres et al. (2013). The short-lived events within GS-24 and GS-22 are not included in the GI and GS duration estimates. Climate changes superimposed to millennial-scale variability are highlighted by the yellow rectangles.

CPD
10, 2595–2626, 2014